THE JOURNAL OF PHYSICAL CHEMISTRY B

Article

pubs.acs.org/JPCB

Mixing Properties of Sphingomyelin Ceramide Bilayers: A Simulation Study

Rainer Metcalf and Sagar A. Pandit*

Department of Physics, University of South Florida, Tampa, Florida 33620, United States

Supporting Information

ABSTRACT: Ceramide is the simplest molecule in the class of glycosphingolipids composed of a sphingosine backbone and acyl moiety. It plays significant roles in cell signaling; apoptosis; binding of hormones, toxins, and viruses; and many other biologically important functions. Sphingomyelin, ceramide with a phosphotidylcholine headgroup, is another biologically vital lipid present in the myelin sheath of nerve cell axons. Regions with high concentrations of ceramide can be formed in biological membranes composed of sphingomyelin by enzymatic catalysis with sphingomyelinase. To better understand the biophysical and thermodynamic properties of these molecules and their mixtures, we have preformed NPT molecular dynamics simulations of hydrated 16:0 sphingomyelin bilayers with increasing concentrations of 16:0 ceramide at 323, 332, 340, and 358 K. From analyses of electron densities, hydrogen bonding, NMR order parameters, partial molecular volume, and partial molecular area, we have identified possible structural changes corresponding to liquid ordered and liquid disordered phases. These structural changes are the results of changes in intra- and intermolecular hydrogen bonds between SM and Cer molecules. Our results correspond to DSC experiments for sphingomyelin bilayer concentrations up to 50% Cer. Above 50% concentration, we observe conformational changes in the SM headgroup similar to that of the umbrella model for lipid cholesterol mixtures.

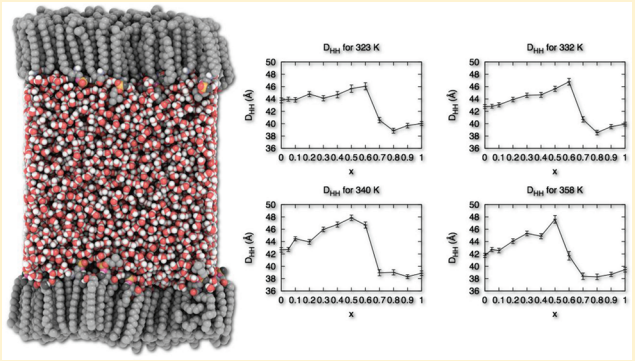

INTRODUCTION

Ceramide (*N*-acyl α-hydroxylated sphingosine) has become a considerable topic of study after it was discovered to be an important signaling molecule.[1−4] The biological significance of ceramide (Cer) includes its roles in the binding of hormones, toxins, and viruses;[5−7] as secondary messengers in signaling pathways;[1] and in apoptosis.[8−10] Cer is derived from the aliphatic amino alcohol sphingosine ((2*S*,3*R*,4*E*)-2-amino-4-octadecene-1,3-diol) and is the hub of sphingolipid metabolism.[11] It is present in relatively diffuse amounts in cell membranes, except for the stratum corneum, where the largely nonpolar molecule also serves as a structural component in membranes. Cer decreases permeability in these membranes, effectively "waterproofing" the epidermis.[12] Cer-rich ordered domains of increased order and rigidity are also implicated in many other diverse biological functions.[13,14]

Sphingomyelin (SM) is another type of glycosphingolipid closely related to ceramide. SM consists of a Cer unit with an esterified phosphorylcholine moiety. The amide-linked acyl chains are usually saturated or monounsaturated and contain 14−24 carbons.[15] SM is a major component of the myelin sheath that surrounds nerve axons. These membranes act as insulators, facilitating action potential across the nerve membrane by inhibiting ion dissipation into surrounding media.[16] Demyelinating diseases such as multiple sclerosis, Guillain−Barr syndrome, and leukodystrophy are thought to originate from the deterioration of these membranes.[17]

Cer can be created from the degradation of SM. This reaction is mediated by the enzyme sphingomyelinase, which causes a hydrolysis reaction with the phosphodiester bond of SM, yielding phosphocholine and Cer. Some potent inducers of sphingomyelinase activity are proinflammatory cytokines, such as tumor necrosis factor-α (TNF-α), interleukin-1β (IL-1β), interferon-γ (IFN-γ), and bacterial lipopolysaccharides.[18,19] Studies done by Singh et al.[20] have also found that reactive oxygen species, such as hydrogen peroxide, can cause degradation of SM membranes in astrocytes, oligodendrocytes, microglia, and glial cells. This leads to the creation of significant quantities of Cer, 18−25% sphingomyelin conversion to Cer, that accumulate in the membrane, leading to death of the cells. Clearly, Cer and SM are important biological molecules.

Cellular metabolism is significantly affected by the structural properties of bilayers composed of these lipids. NMR experiments by Huang et al.[21] have shown that the addition of Cer to dipalmitoylphosphatidylcholine (DPPC) membranes at 45 °C induced lateral phase separation of the bilayers into regions of gel and liquid crystalline phases. The author reasoned this effect was due to packing defects in the bilayer. NMR studies performed by Thewalt et al.[22] also showed that complex mixing

Received: December 21, 2011
Revised: March 2, 2012
Published: March 5, 2012

behavior arose when Cer was introduced to sphingomyelin bilayers. It was suggested that,[14,23,24] despite being structurally different from cholesterol (Chol), the rigidity of long-chain Cer is similar to the rigidity of the sterol rings of Chol. This combination gives rise to detergent-resistant membrane regions of increased lipid chain order. Xu et al.[25−27] observed that Cer stabilizes domain formation in SM and other phosphocholine lipid mixtures with Chol. It was also noted that Cer displaces Chol from those domains. Further, the authors suggest that tight lipid chain packing is essential for sterol displacement by Cer. This packing behavior also prevents unfavorable contacts between lipid hydrocarbon chains and water. Recent studies have also shown that, depending on the Chol/Cer ratio, Chol can displace Cer, as well, and influence the generation and distribution of SM/Cer domains.[28] Deuterium NMR studies by Hsueh et al.[29] found that domains of gel and liquid-crystalline phases coexist in mixtures of palmitoyloleoylphosphocholine (POPC) and Cer over a wide range of temperature and compositions above 15 mol % Cer. These experiments give rise to the idea that the effect of Cer on lipid chain packing in low concentrations exhibits properties similar to that of Chol.[30]

Simulations consisting of these lipids and their mixtures are useful in elucidating underlying interactions between Cer and SM. Insights gleaned from these interactions can then be connected to their biological activity. Molecular dynamics (MD) simulations performed by Chiu et al.[31] showed the dynamics of SM systems are distinctly different from those of a DPPC bilayer. The authors also remarked on the relative lack of experimental and computational studies done on these biologically important mixtures of SM. Zhang et al.[32] suggested that phase separation was closely linked to the balance of energy and entropy change when mixing SM, POPC, and Chol. Pandit et al.[30] proposed through MD simulations that Cer may, under some circumstances, act as a surrogate for Chol and may also be an evolutionary precursor to it.[33] As described above, because of the ease of accumulation of Cer via enzymatic catalysis of SM, comparisons of structural effects of Cer on SM bilayers are important in understanding the mechanisms of some diseases and the biological effects of these molecules and their mixtures.

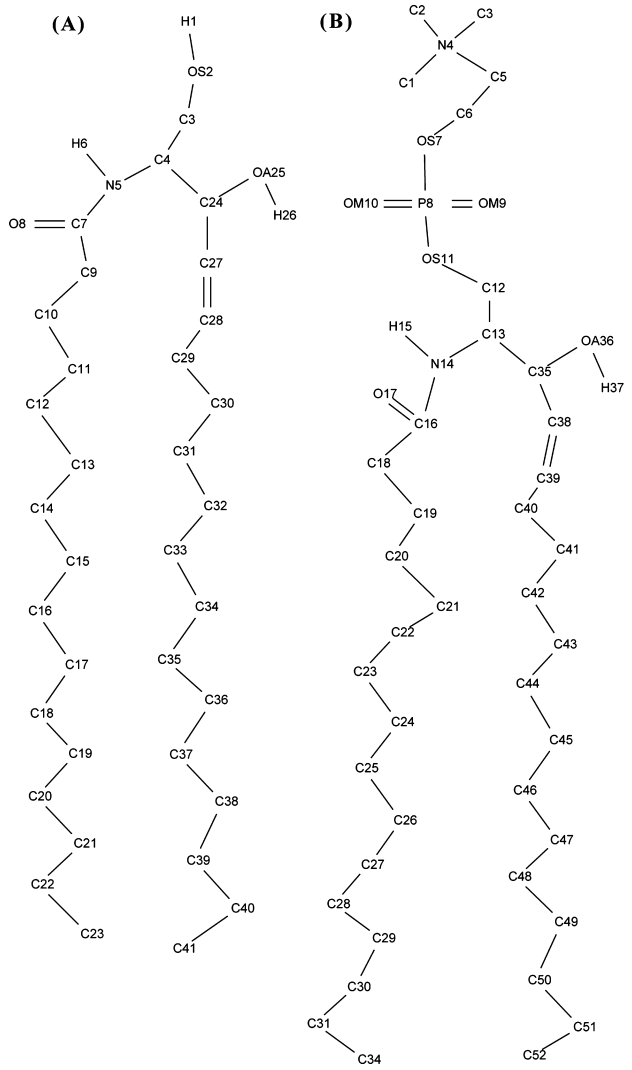

Figure 1. Structures of palmitoyl 16:0 Cer (A) and palmitoyl 16:0 SM (B). Molecules shown with atom names.

METHODS

The MD simulations were performed on hydrated 16:0 SM bilayers with varying concentrations of 16:0 Cer ranging from 0 to 100% at 10% increments. In addition, simulations with 5% concentrations of Cer were also preformed for better sampling of concentration. Figure 1A and B shows the structure of the Cer and SM molecules respectively, along with the associated atom names. The force-field parameters used for the SM and Cer molecules were taken from previous work.[24,31] Our systems were simulated at four different temperatures—323, 332, 340, and 358 K—using the Nose−Hoover temperature coupling scheme .[34] Each system consisted of 200 lipids with appropriate proportion of SM and Cer molecules. The systems were hydrated with 20 000 SPC/E water molecules. This ensured a lipid water ratio of 1:100. This translates to ∼71.9 wt % water for pure SM and ∼83.7 wt % water for pure Cer. The amount of water used in these simulations was adequate because a Cer bilayer is considered fully hydrated at 74.3 wt % water or a lipid water ratio of 1:86.[35]

These simulations were performed using the GROMACS package, version 3.3.[36,37] The linear constraint solver LINCS algorithm was used to constrain all bonds in the system,[38] allowing an integration time step of 2 fs. Periodic boundary conditions were applied in all three dimensions, and long-range electrostatics were calculated using the SPME algorithm[39] with a real-space cutoff of 9.5 Å. A cutoff of 16 Å was employed for van der Waals interactions. The systems were simulated in an NPT ensemble using the Parrinello−Rahman pressure-coupling scheme at a constant pressure of 1 atm.[40]

Initial configurations for all the mixture systems were generated by random placement of 100 bilayer molecules per leaflet in appropriate proportion such that the lipids were aligned along the z axis and the hydrocarbon chains were pointing toward the z = 0 plane. Two blocks of 10 000 SPC/E waters were placed above and below the constructed bilayers. The systems were energy-minimized to remove bad contacts resulting from overlapping hard sphere surfaces and over stretched bonds. All the systems were annealed to ensure proper thermalization of the hydrocarbon chains. The annealing steps involved raising the initial temperature of the systems to 600 K and lowering it by steps of 50 K per 250 ps until the systems reached the desired temperatures. After the annealing process, 30 ns continuous MD simulations were performed on each system. The box areas and volumes were monitored throughout the duration of the simulations. All analyses were performed on the last 10 ns of each

dx.doi.org/10.1021/jp212325e | J. Phys. Chem. B 2012, 116, 4500−4509

Table 1. Table of Comparisons for Pure SM Systems

quantity	temperature, K	results	Niemela et al.[43]	Chiu[a] et al.[31]	Mehnert et al.[46]
area per lipid (Å^2)	323	53.3 ± 0.4	52 ± 1	53	
volume per lipid (Å^3)	323	1167.8 ± 12.1	1180 ± 10	1182	
D_{HH}	323	43.8 ± 0.3	43.4 ± 0.5	42.4	
S_{CD}	321				0.221
	323	0.246	0.26	0.25	

[a]Simulations performed with 18:0 SM.

simulation where fluctuations in the box areas and volumes were minimal.

Pandit et al.[41] have reported the inaccuracies in measurements of volumetric properties of mixed bilayers for short time scale simulations (i.e., less than 50 ns). These inaccuracies stem from the changes due to slow lateral molecular diffusion in mixed lipid bilayers. However, for the simulations reported here, the area per molecule and lateral mean square displacement begin to equilibrate around 20 ns. From the previous author's data, this yields a possible error in the area per molecule. Our analyses are based on a comparison between systems, and therefore, any systematic error is expected to change quantitative results by up to a constant. Thus, these simulations provide accurate qualitative description of lipid mixing. Much larger systems and longer run times may be necessary to obtain a more comprehensive quantitative measure of lipid mixing.

RESULTS

Validation of the Simulations. The simulations were validated first by comparing the structural properties of the simulated systems with the experimental and previously reported simulation studies. The systems with 0% and 100% Cer were used for this purpose.

Tables 1 and 2 show the structural properties for pure SM in this and previous works. To the best of our knowledge, there are few experimental studies that report area per lipid for pure SM systems. Further, inherent difficulty in determining accurate area per lipid creates varied and sometimes incompatible results for comparison.[42] Hence, we relied primarily on previous simulation studies for comparisons. Our computed average area per lipid for pure SM was found to be 53.3 ± 0.4 Å^2, which is in agreement with simulation values, reported by Niemela et al., of 52 ± 1 Å^2.[43] Simulations on SM bilayers performed by Chiu et al.[31] reported area per lipid for 18:0 SM as 53 Å^2. The simulation performed by these authors used a much larger membrane of 1600 lipids. This larger membrane allowed for more significant effects caused by undulations of the bilayer. Table 2 shows comparisons of intermolecular hydrogen bonds of SM with previous simulation studies by Khelashvili et al.[44] Interlipid hydrogen bonds between various donor and acceptor sites displayed reasonable agreement with their simulation. Hydrogen bonds between SM and water showed a similar concurrence.

Table 2. Comparisons of Average Number of Hydrogen Bonds for Various Donor/Acceptor Sites of Pure SM

donor/acceptor	atom pair	coordination number results	Khelashvili et al.[44]
SM−water	OM9 or OM10−HW	1.11	1.14
SM−water	OS7−HW	0.60	0.49
SM−water	OS11−HW	0.19	0.24
SM−water	OA36−HW	0.94	0.93
intermolecular (SM)	O17−H15	0.32	0.30
intermolecular (SM)	OA36−H15	0.18	0.11
intermolecular (SM)	H37−OS11	0.77	0.57
intermolecular (SM)	H37 − OS7	0.03	0.02

Using the method described by Petrache et al.,[45] the average volume per lipid for SM at 323 K was calculated to be 1168 ± 12 Å^3 and is within error of average volume per lipid calculations of 1180 ± 10 Å^3 for 16:0 SM and 1182 Å^3 for 18:0 SM from Niemela et al. and Chiu et al., respectively.[31,43] Peak-to-peak distance calculated from electron densities reported from Niemela et al. and Chiu et al. were in excellent agreement with our computed values[31,43](Table 1). Further, we note that the average deuterium order parameter for acyl chains was comparable to previous simulation results. Experimental NMR order parameters for 16:0 SM bilayers at 321 K by Mehnert et al.[46] found an average acyl chain order parameter, $\langle S_{CD} \rangle$, of ∼0.221, compared with our result of $\langle S_{CD} \rangle$ = 0.246 ± 0.022. Comparison of order parameter profiles from our simulations closely matches profiles from previous simulations.[31,43]

There are a limited number of studies on pure Cer bilayers reported in the literature, thereby making validation difficult and limiting the number of conclusions that can be drawn from our data. Differential scanning calorimetry experiments by Shah et al.[35] on pure 16:0 Cer bilayers found a broad exothermic transition between 328 and 343 K with no exothermic transition in cooling run.[35] This indicated an irreversible transition from a metastable lamellar phase to a stable bilayer. For a fully hydrated bilayer, this transition occurred at 337.2 K. The X-ray diffraction data from Shah et al.[35] showed a lamellar repeat distance of 41.8 Å and noted a significant drop in the lamellar repeat distance after the phase transition. Our peak-to-peak distance showed a drop of ∼1.3 Å between the temperature of 332 and 340 K. Order parameters also exhibited an overall decrease of ∼0.03 for a similar change in temperature and with a corresponding ∼1.6 Å^2 increase in area per lipid. Thus, our simulations are successful in reproducing qualitative behavior of a pure Cer bilayer over a wide range of temperatures that encompass a phase transition.

Mixing Properties of the Lipids. Several structural measures can be used to ascertain the mixing behavior of the lipids in bilayers. Our analyses include studies of PMV, PMA, electron densities, and order parameters.

Partial Molecular Volume and Area. Determination of partial molecular volume (PMV) is an effective way of ascertaining the equation of state for heterogeneous liquids. Following Greenwood et al.,[47] the PMV and partial molecular area (PMA) of the bilayers were investigated. According to the standard definition of PMV, the total volume, $v(N_{Cer}, N_{SM})$, as a

dx.doi.org/10.1021/jp212325e | J. Phys. Chem. B 2012, 116, 4500−4509

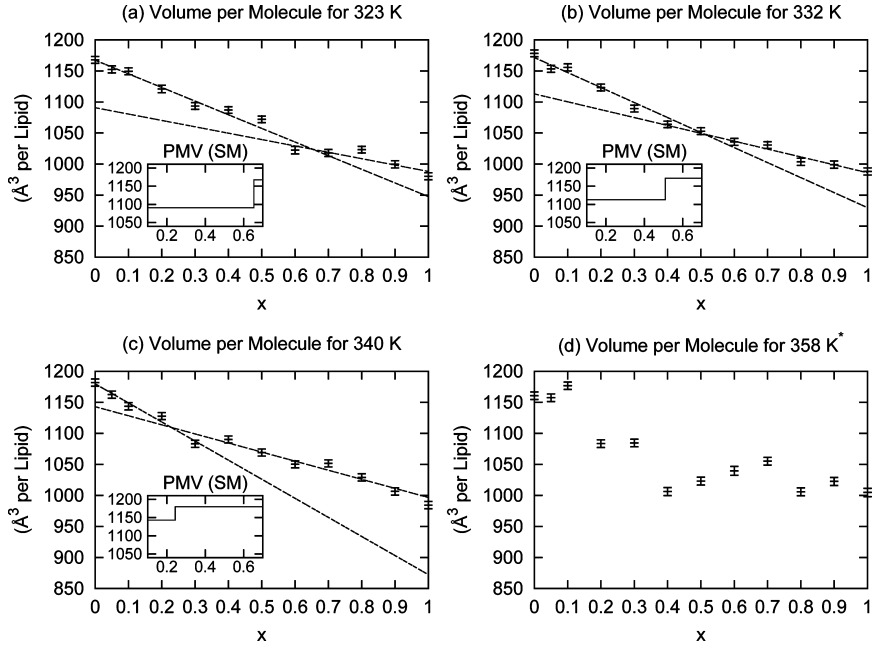

Figure 2. Plots of volume per lipid with respect to concentration, x, of Cer. Intersecting linear fits (dashed lines) represent discontinuous changes in slope shown as insets. The slopes of the linear fits correlate to the partial molecular volume of SM. Discontinuities in PMV shifted to lower concentrations for higher temperatures. *Systems for 358 K did not yield reliable linear fits and so PMV was not calculated for these systems.

function of Cer concentration, x, for the binary mixture can be expressed as a linear relationship,

$$v(N_{\mathrm{Cer}}, N_{\mathrm{SM}}) = x\nu_{\mathrm{Cer}} + (1 - x)\nu_{\mathrm{SM}} \tag{1}$$

where ν_{Cer} and ν_{SM} are the PMVs for Cer and SM, respectively. Differentiating eq 1 yields a set of linear equations that can be solved to obtain PMVs as

$$\nu_{\mathrm{Cer}} = v(x) + (1 - x)\frac{\mathrm{d}v(x)}{\mathrm{d}x} \tag{2}$$

$$\nu_{\mathrm{SM}} = v(x) - x\frac{\mathrm{d}v(x)}{\mathrm{d}x} \tag{3}$$

Figure 2 displays lipid volume as a function of x, where extraction of the lipid volume from total box volume was performed using the method proposed by Petrache et al.[45] We note from Figure 2 that, for most cases, the dependence of the lipid volume on x is a piecewise linear function. Thus, the derivatives in eqs 2 and 3 were calculated by computing the slopes of these fitted functions. The inset graphs of Figure 2 show PMV for SM as a function of x. For the values of x between 0.3 and 0.6, ν_{SM} exhibits discontinuities with an overall decrease in PMV. Figure 2d at 358 K did not yield reliable linear or piecewise linear fits. Therefore, ν_{SM} was not computed in this case. Further, as a function of temperature, these discontinuities shift to lower concentrations and are more prominent. Any discontinuity in PMV correlates to volumetric effects in a system due to either chemical reactions or structural rearrangements of the molecules.[47,48] Classical MD does not incorporate chemical interactions; therefore, structural rearrangements and conformational changes of the lipids must be the cause of any change in PMV.

For two-dimensional liquids such as lipid membranes, area per lipid is considered approximately an extensive quantity similar to the volume.[48] Hence, one can introduce PMA by essentially replacing volume with area in the volume derivation. Following analysis of Figure 2, we investigated the behavior of PMA (Figure 3). Similar to PMV, the region between $0.1 \leq x \leq 0.6$ exhibited a discontinuous decrease in PMA. This discontinuity shifted to higher concentration with increasing temperature. We note that the reduction in PMA was very similar to that of lipid cholesterol mixtures.[41,48] This behavior implies that the presence of Cer induced structural changes in lipid bilayers comparable with those of Chol and may serve as a surrogate for Chol in this region.[30]

Deuterium Order Parameters. Structural changes in lipid membranes are correlated to the degree of disorder in hydrocarbon chains. This disorder is quantified in NMR experiments by measuring deuterium order parameter profiles. The order parameter tensor, S, is defined as

$$S_{ab} = \frac{1}{2}\langle 3\cos(\theta_a)\cos(\theta_b) - \delta_{ab}\rangle \qquad a, b = x, y, z \tag{4}$$

where θ_a is the angle made by the ath molecular axis with the bilayer normal and δ_{ab} is the Kronecker delta. In simulations with united atom force fields, the order parameter for saturated and unsaturated carbons, S_{CD}, can be determined using the following relations:[49]

$$-S_{\mathrm{sat}}^{\mathrm{CD}} = \frac{2}{3}S_{xx} + \frac{1}{3}S_{yy} \tag{5}$$

$$-S_{\mathrm{unsat}}^{\mathrm{CD}} = \frac{1}{4}S_{zz} + \frac{3}{4}S_{yy} \mp \frac{\sqrt{3}}{2}S_{yz} \tag{6}$$

Figure 4 shows the deuterium chain order parameters averaged over the entire length of the acyl chain (Figure S1 in the Supporting Information). Average sphingosine chain order parameters (Figure S4 in the Supporting Information), calculated from Figure S2 in the Supporting Information, showed similar trends. Careful observation of these figures illustrates that the chain order increases with an increasing

dx.doi.org/10.1021/jp212325e | J. Phys. Chem. B 2012, 116, 4500−4509

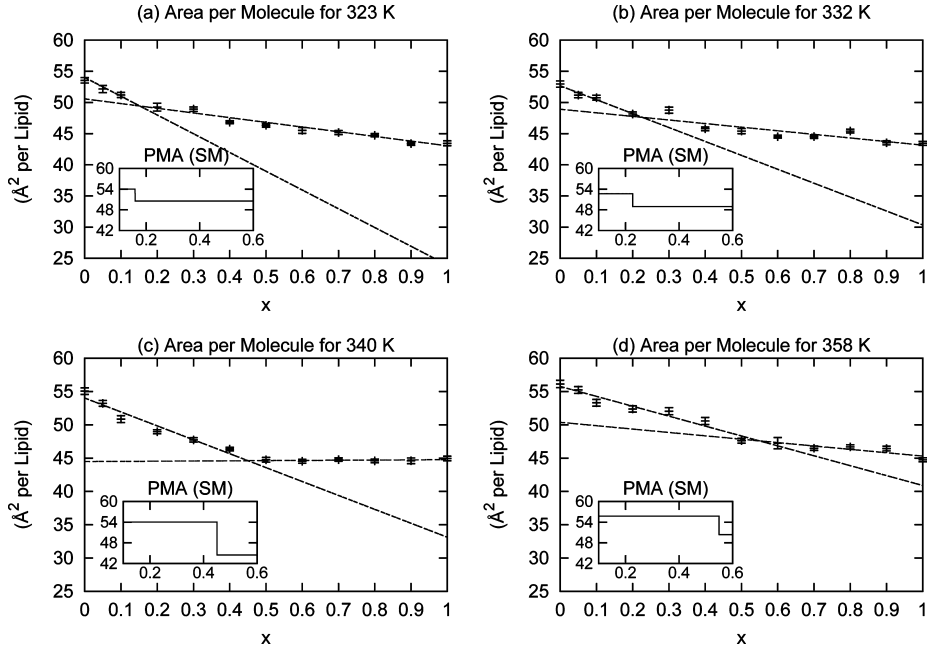

Figure 3. Plots of area per lipid versus *x*. Intersecting linear fits (dashed lines) represent discontinuous changes in slope shown as insets. The slopes of the linear fits correlate to the partial molecular area of SM. Discontinuities in PMA were shifted to higher concentrations for increasing temperatures.

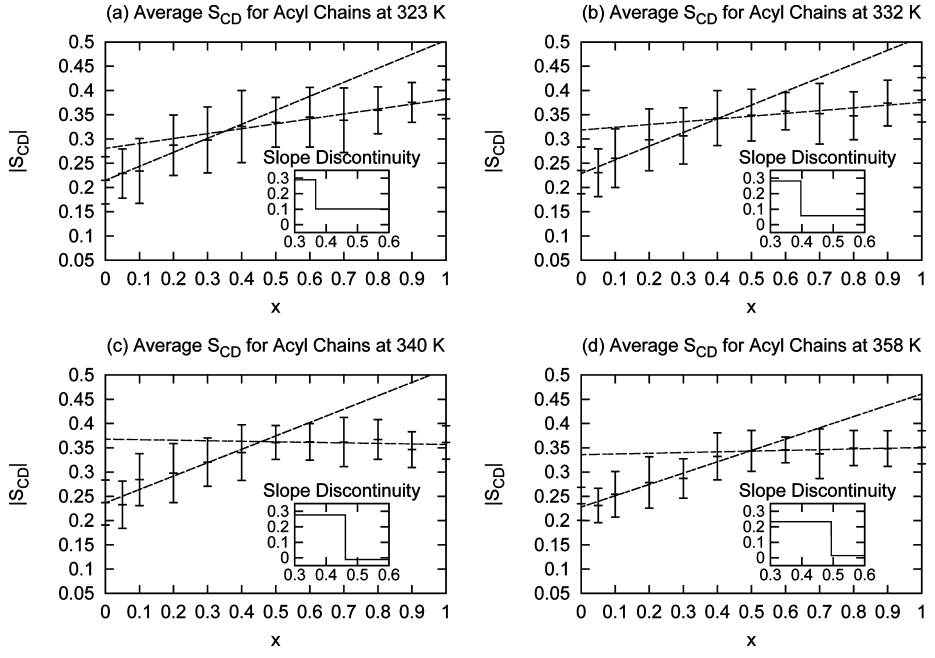

Figure 4. Average palmitoyl acyl chain order for both Cer and SM molecules as a function of concentration, *x*. Order parameters were averaged over the entire length of the chain. Discontinuity in linear fits (shown in inset) denote possible structural changes. These discontinuities have trends similar to that of PMA. Note that the insets show the derivative of order parameters with respect to Cer concentration, not the actual order parameter values.

concentration of Cer. The rate of change of the order parameter with respect to *x*, plotted as insets, displays discontinuity. This behavior is indicative of Cer's ordering SM bilayers more effectively at lower concentrations than at higher concentrations. Further, these discontinuities shift toward higher values of *x* with increasing temperature. This change in order corresponds to similar changes observed in PMA analysis (Figure 3). Discontinuities in the order parameters of sphingosine chains (Figure S4 in the Supporting Information) fluctuate between 0.4 and 0.5 concentrations. Therefore, it can be concluded that the effect of Cer appears to be more prominent on the acyl chain than the sphingosine chain.

Electron Densities. Electron density profiles can also reveal structural properties of a bilayer through analysis of membrane thickness, leaflet symmetry, and lipid packing behavior. These structural analyses can then be correlated to chain order, PMA, and PMV. In experiments, the structure factor of the bilayer is

dx.doi.org/10.1021/jp212325e | J. Phys. Chem. B 2012, 116, 4500–4509

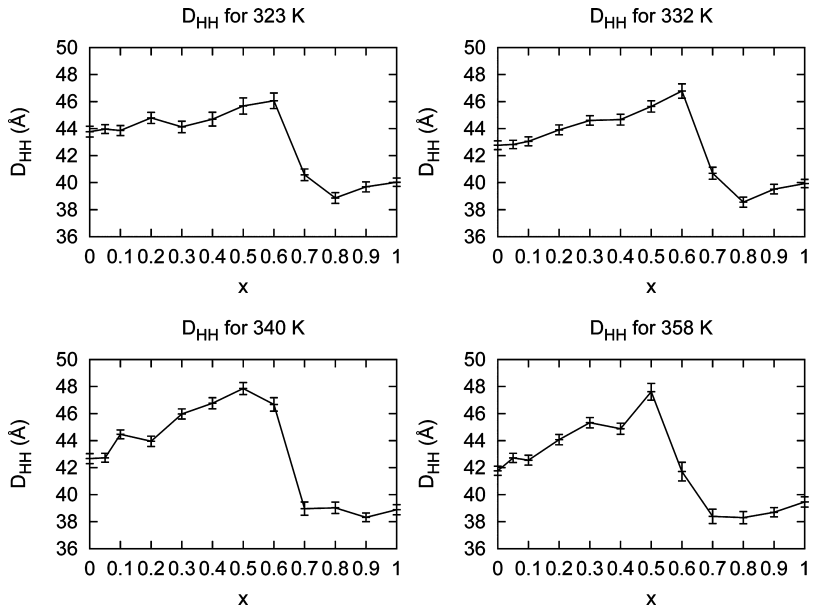

Figure 5. Peak to peak distance in electron density (D_{HH}). Peaks in electron density correspond to the phosphate groups in the head groups of SM in each leaflet. A pronounced decrease occurs at 50 and 60% concentration Cer for all systems.

obtained from X-ray diffraction patterns. The electron density profile is then deduced from the structure factor.[42] In simulation studies, the positions and partial charges of the atoms are known, thereby allowing direct computation of the electron densities. As expected, electron densities show a trough at the center of the hydrocarbon core and prominent peaks corresponding to the phosphate groups (Figure S3 in the Supporting Information). The distance between these peaks (D_{HH}) is a measure of bilayer thickness (Figure 5). This figure shows gradual thickening of the bilayer with increasing concentration of Cer. This phenomenon is consistent with the corresponding increase in the order parameters and decrease in PMA. All graphs show abrupt reduction in thickness at intermediate concentrations. This thickness reduction occurs at slightly lower concentration ($x \approx 0.6$ to $x \approx 0.5$) for higher temperatures, 340 and 358 K. The shift in the peak to peak distance appears to have a concentration dependence similar to that of PMV analyses. Since steep reduction in the peak to peak distance cannot be attributed to the smaller volume of Cer alone, the reduction in thickness may be due to possible "tilting" of hydrocarbon chains and/or the configuration of the SM headgroup.

Head Group Orientation. The phosphate group in the SM choline headgroup is, to a significant degree, the most electron dense region of the SM molecule. The position of this phosphate group in the membrane greatly influences the locality of peak electron density. Conformational changes in SM headgroup tilt were quantified by computing the average angle between the bilayer normal and the vector joining the sphingosine C13 backbone carbon to the P8 phosphorus atom (Figure 6A). The figure clearly shows an increase in headgroup tilt with increasing Cer concentration. We note that the tilt angle is largely independent of temperature and alludes to a relationship to Cer concentration consistent with observed decreases in D_{HH}.

Head Group–Water Interaction. The change in headgroup orientation may be correlated to a decrease in bound waters surrounding the choline headgroup. Dehydration of SM headgroup may also have an effect on D_{HH} which is a distance between peak electron densities of each leaflet. These electron densities are a superposition of lipid and water densities. Analysis of bound water was performed by calculating radial distribution functions (RDF) of SM head groups with the oxygen atom in water. The average number of bound waters is displayed in Figure 6B. This figure shows an initial hydration of ≈3.5 waters per headgroup for pure SM, followed by a mainly linear decrease in the number of bound waters per SM headgroup with respect to Cer concentration. Recent neutron diffraction studies by Ryabova et al.[50] have shown that the incorporation of Cer and Chol into DPPC bilayers increases bilayer thickness by affecting membrane hydration. In addition, the authors noted that Cer, in contrast to Chol, significantly reduces the thickness of the membrane water layer. The effects observed by Ryabova et al.[50] for DPPC bilayers may have correlations similar to SM–Cer mixtures in our systems. The dehydration of SM bilayers with increasing concentrations of Cer is also consistent with observed reductions in hydration of the stratum corneum due to Cer formation by sphingomyelinases.[51]

DISCUSSION

Combining analyses of PMV, PMA, average S_{CD}, and D_{HH}, we observe emergence of rich and complex mixing behavior in SM–Cer systems. Through enzymatic catalysis of SM, large concentrations of Cer can collect in cellular membranes. Thus, the previously mentioned emergent behavior of these systems may be critical in elucidating mechanisms of some diseases and the biological effects of these molecules and their mixtures. Throughout this work, we evaluated discontinuous changes in observed quantities. Due to finite size and short duration of our simulations, these discontinuities may or may not correspond to thermodynamic phase change; however, in our opinion, these are qualitative indicators of such phenomena.

We observed two distinct correlations based on the six quantities computed in these simulations. Acyl chain S_{CD} (Figure 4) and PMA (Figure 3) display some equivalent proclivity of discontinuities' shifting toward higher values of x with increasing temperature. On the other hand, PMV (Figure 2), headgroup hydration, and D_{HH} (Figure 5) show correlations and are contradistinguished to PMA and acyl chain S_{CD}. These trends are summarized in Figure 7. As noted in previous sections, PMA demonstrates the condensing effect of Cer in SM

dx.doi.org/10.1021/jp212325e | J. Phys. Chem. B 2012, 116, 4500–4509

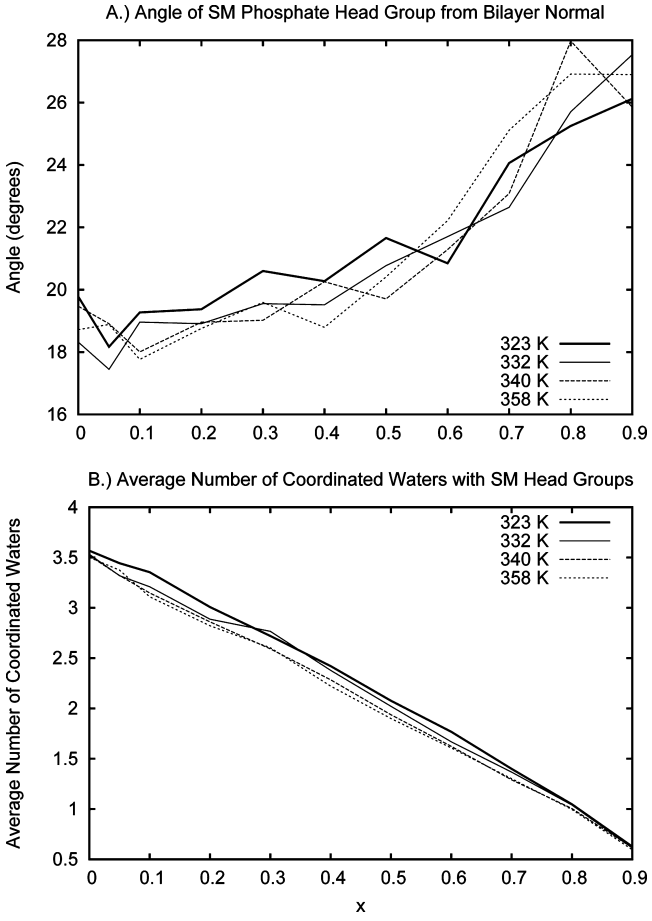

Figure 6. (A) Angle of SM phosphate headgroup from bilayer normal. Angle calculated by vector drawn from C13 backbone carbon to P8 phosphorus atom. Figure shows a general increase in angle for concentrations above $x = 0.5$, with little temperature dependence. (B) Average number of coordinated waters per SM headgroup. Coordination numbers from RDF of SM headgroup with oxygen from water are correlated to show hydration effects of the addition of Cer on SM bilayers. Mainly linear decreases are observed over all concentrations.

bilayers resembling that of Chol. This condensing effect is attenuated at certain concentrations. The loci of these concentrations on a temperature plot demarcate regions of chain orders consistent with separation of liquid disordered and liquid ordered phases. Similar ranges in concentration and temperature have been shown to have enthalpic phase transitions and changes in detergent resistance in experiments performed by Busto et al.[52] (shown as a comparison in Figure 7). The DSC curve in Figure 7 was based on the approximate position of peaks in DSC data by Busto et al. (Figure 7 of Busto et al.[52]). It is important to mention that line fitting has inherent inaccuracy due to noise in the fitted data. The actual points shown in Figure 7 are qualitative indicators of structural change and should not be taken as exact "phase" boundaries.

Hydrogen bonding networks were also analyzed and showed some preferential intermolecular orientations (Table 3). The SM OA36 and H37 hydroxyl group displayed an almost exclusive intermolecular affinity to the OS11 oxygen ester (row 18 of Table 3). The N14 amide group in the sphingosine base evinced a propensity to the acyl chain O17 carbonyl group (row 15 of Table 3). The preferential nature of these intermolecular SM bonds was disrupted by the addition of Cer. In

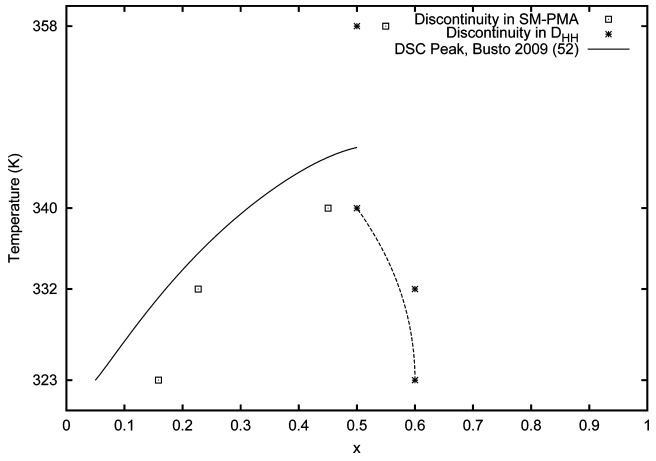

Figure 7. Prominent structural changes generated by combining points of discontinuity from linear fits of PMV, PMA, order parameters, and peak-to-peak electron densities. For clarity, only PMA (squares) and D_{HH} (dashed line) are shown. Solid line represents inferred trendline in discontinuities of DSC experiments by Busto et al.[52]

particular, intermolecular SM N14 hydrogen bonds were displaced by an increased affinity for oxygen groups in Cer (rows 7, 8, 17, and 19 of Table 3).

Similar bonds in Cer do not show the same structural propensities as that of SM. The OA25 and H26 hydroxyl group showed a slightly increased association with the O8 acyl chain carbonyl group over the N5 sphingosine amide group (rows 12 and 14 of Table 3). The SM N4 quaternary amide group and OM9 and OM10 phosphate oxygens did not play a significant role in interlipid hydrogen bonding. This is contrary to the OS2 headgroup of Cer, which did display significant intermolecular hydrogen bonds with other Cer molecules. At concentrations higher than $x = 0.4$, the Cer N5 amine group showed a substantial increase in affinity for the Cer O8 carbonyl group and a smaller increase for the Cer OA25 and H26 hydroxyl group (rows 12 and 13 of Table 3). Hydrogen bonds between Cer and SM showed a large degree of fluctuation but did not display any considerable dependence on concentration. Hydrogen bonds for all of our systems exhibited a general insensitivity to temperature. Thus, analysis showed some preferential configuration for SM molecules due to hydrogen bonds between the hydroxyl group and ester group and between the amide group and carbonyl group. These hydrogen bonding patterns were disrupted with increasing Cer concentration. On the other hand, the hydroxyl headgroup of Cer played a far more significant role in intermolecular hydrogen bonding. The hydrogen bonding patterns showed a distinct preference for molecules of the same type (i.e., SM with SM and Cer with Cer).

To the best of our knowledge, the seminal works by Busto et al. are the only experimental results published on bilayers with bimodal mixtures of SM and Cer. Unfortunately, their experiments incorporate Cer concentrations of only up to 50%. In our simulations, a gradual increase in D_{HH} is seen for lower concentrations, followed by a significant decrease of ≈8 Å occurring at concentrations of $x \geq 0.5$ (Figure 5). The gradual increase is expected because of the ordering of the hydrocarbon chains. At concentrations higher than $x = 0.5$, a saturation point is observed in which the further addition of Cer no longer increases chain order (Figure 4 and Figure S4 in the Supporting Information). The noted decrease in D_{HH} is correlated to an increase in the headgroup angle away from the membrane

dx.doi.org/10.1021/jp212325e | J. Phys. Chem. B 2012, 116, 4500–4509

Table 3. Hydrogen bonds for various donor and acceptor sites

			coordination number for various concentrations					
row	donor/acceptor	atom pair	0	5	10	50	70	100
1	SM−Cer	OS7−OS2		0.01	0.01	0.06	0.02	
2	SM−Cer	OS11−OS2		0.02	0.13	0.12	0.08	
3	SM−Cer	OM9 or OM10−OS2		0.12	0.08	0.05	0.08	
4	SM−Cer	O17−OS2		0.07	0.17	0.09	0.08	
5	SM−Cer	OA36−N5		0.04	0.20	0.13	0.10	
6	SM−Cer	O17−N5		0.45	0.24	0.26	0.14	
7	SM−Cer	N14−OA25		0.20	0.11	0.08	0.18	
8	SM−Cer	N14−O8		0.52	0.33	0.27	0.40	
9	intermolecular (Cer)	OS2−OS2		0.01	0.04	0.09	0.14	0.13
10	intermolecular (Cer)	OS2−OA25		0.46	0.45	0.44	0.52	0.54
11	intermolecular (Cer)	OS2−O8		0.01	0.04	0.03	0.06	0.08
12	intermolecular (Cer)	N5−OA25		0.02	0.01	0.11	0.18	0.24
13	intermolecular (Cer)	N5−O8		0.02	0.04	0.40	0.34	0.57
14	intermolecular (Cer)	OA25−O8		0.47	0.42	0.40	0.43	0.41
15	intermolecular (SM)	O17−N14	0.32	0.38	0.35	0.23	0.10	
16	intermolecular (SM)	O17−OA36	0.15	0.13	0.14	0.13	0.20	
17	intermolecular (SM)	OA36−N14	0.18	0.17	0.20	0.09	0.05	
18	intermolecular (SM)	OA36−OS11	0.77	0.77	0.82	0.84	0.71	
19	intermolecular (SM)	OA36−OS7	0.03	0.02	0.03	0.01	0.01	

normal. The increase in the headgroup angle also corresponds to a decrease in bound waters surrounding the SM head groups. This may indicate that the SM headgroup is collapsing toward the center of the membrane as a result of the dehydration of the SM headgroup. The drop in PMV may be also be caused by the deflection of the SM headgroup toward the bilayer center. From the comparisons of these quantities, we may be able to infer that for concentrations of $x \geq 0.5$, the effect of SM headgroup dehydration on D_{HH} surpasses the chain ordering effects of Cer. Experimental results for concentrations above 50% Cer are necessary to verify this observed phenomenon.

Another possible mechanism for the marked decrease in D_{HH} was proposed for pure Cer bilayers by Shah et al.[35] They observed that Cer formed a metastable bilayer with straightened hydrocarbon chains that transitioned into a more stable state. Further, they conjectured that this observed transition was caused by the "tilting" of the Cer molecule away from the membrane normal axis. The overall order parameters should be uniformly shifted as a result of such "tilting" behavior. Careful review of the order parameter profiles (Figures S1 and S2 in the Supporting Information) did not exhibit any statistically significant shift. Analysis of the angle formed by the vector from the backbone C13 carbon and terminal acyl methyl groups with the bilayer normal also showed no evidence of this proposed mechanism (data not shown).

The apparent discrepancy between the reduction in D_{HH} and no significant reduction in PMV requires careful study of the methods used in computation of lipid volume. We identify three distinct methodologies to compute lipid volumes, namely:

Method 1: The principle method utilized in this study to determine component lipid volumes was a technique proposed by Petrache et al.[45] This procedure details and delineates water volume that can be subsequently subtracted from the total volume to leave only the total lipid volume. Partial molecular volumes of the component lipids can then be determined. This method is ideal, in that it does not explicitly assume any details concerning the conformations of the lipids in the bilayer.

Method 2: Combining membrane area calculations with D_{HH} is another common method of procuring volume data. An estimation of the z axis component of the bilayer can be done using D_{HH} to define membrane thickness. Volume can then be defined as $V_L = D_{HH} \times A/2$. This procedure does assume the lipids are in a straightened orientation in the bilayer and that any deviation from the assumed cylindrical form by conformational changes would cause the z component to shift. These conformational changes would also cause the area per lipid to change, as well, thus conserving the total volume.

Method 3: A method similar to method 2 could be devised using the concept of the Gibbs−Luzzati bilayer thickness, D_B, to define a transverse description of the bilayer analogous to D_{HH}.[42] This method defines a region on the z axis where the lipid-atom-to-water ratio is equal to 1. The distance between these points on both leaflets provides an estimation of the bilayer thickness. Volume can then be calculated as $V_L = D_B \times A/2$. Although, like the previous method, this method also assumes cylindrical shape of the molecule, the thickness calculations are not explicitly dependent on specific lipid conformations. The thickness calculations in this case are only a function of the interfacial properties and the hydration structure of the system.

Figure 8 shows computed volumes using these three methods. At lower concentrations of Cer, $x \leq 0.6$, all three methods show a similar linear decrease in volume per molecule in response to replacing SM with Cer. Volume calculations using method 2 display substantial deviation from the other two methods for Cer concentrations higher than $x \approx 0.6$. In method 2, the positions of the phosphate groups in SM primarily determine D_{HH}. Any change in headgroup conformation of SM will be reflected in measurement of D_{HH}. We observe that the SM headgroup tilts away from bilayer normal at higher Cer concentrations (Figure 6A). Such tilt, in a mixed bilayer, may provide a configuration in which reduction in D_{HH} can be achieved without

dx.doi.org/10.1021/jp212325e | J. Phys. Chem. B 2012, 116, 4500−4509

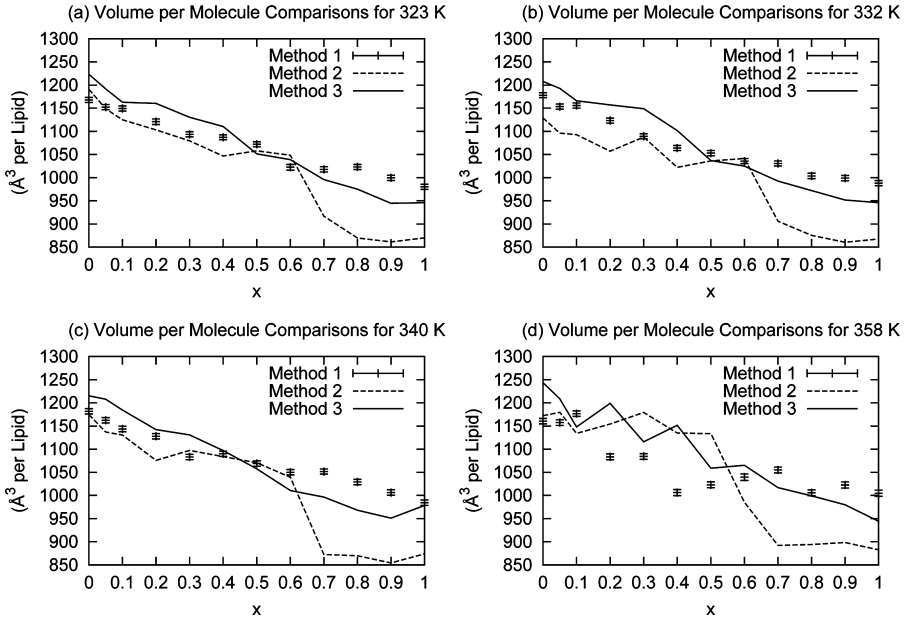

Figure 8. Comparisons of volume per lipid calculations using the method proposed by Petrache et al. (points), $V_L = D_{HH}A/2$ (dashed lines), and $V_L = D_BA/2$ (solid line).

significantly changing area per lipid, thus, reducing the volume by method 2. This mechanism closely resembles the umbrella model introduced by Huang et al.[53] as a possible explanation for the observed solubility of Chol in bilayers.

Simulations at 358 K portray large fluctuations and deviations from fitted data at lower temperatures. These discrepancies may be due to poor performance of the SPC/E water model at high temperatures. Comparison of calculated water density with experimental density values[54] showed diminishing ability of the SPC/E water model to accurately reproduce water densities at relatively higher temperatures (Figure S5 in the Supporting Information). Studies on the thermodynamic properties of water models also show similar effects from SPC/E water at temperatures near boiling point.[55] This leads to the conclusion that possible error in our analyses was due in large part to breakdown of the SPC/E water model at higher simulation temperatures (i.e., 358 K). However, we are confident that our simulation parameters and the SPC/E water model for lower temperatures produce structural properties of our systems with reasonable accuracy.

SUMMARY

We have performed molecular dynamics simulations of hydrated 16:0 sphingomyelin bilayers with increasing concentrations of 16:0 ceramide at 323, 332, 340, and 358 K. To the best of our knowledge, these are the only simulations on Cer−SM systems. Through the analysis of PMA, PMV, average chain order parameters, and electron densities, we have identified regions of significant structural changes. These changes coincide with phase changes observed in DSC experiments. Hydrogen bond analysis showed some preferential configuration for SM molecules as a result of hydrogen bonds between specific chemical groups of SM. These observed affinities are disrupted with increasing Cer concentration. Hydrogen bonding patterns also showed a distinct preference for molecules of the same type. Further, we predict significant structural changes in our systems, associated with the dehydration of the SM headgroup, for Cer concentrations above 50%. We also observe that at higher Cer concentrations, SM head groups tilt toward the bilayer center, forming an "umbrella" over Cer under it. Experimental validation of this phenomenon would provide great insight into the structure and function of these systems.

ASSOCIATED CONTENT

Supporting Information

Additional information as noted in text. This material is available free of charge via the Internet at http://pubs.acs.org.

AUTHOR INFORMATION

Corresponding Author

*E-mail: pandit@usf.edu.

Notes

The authors declare no competing financial interest.

ACKNOWLEDGMENTS

We thank Pranali Dalvi for contributions in monitoring simulations and Dr. Gauri Pradhan for valuable commentary. This work was supported in part by the University of South Florida Office of Research & Innovation through the New Researcher Grant Program under Grant No. R066395, and National Institute of Health Grant No. 1R01GM086707-01A1.

REFERENCES

(1) Futerman, A. H.; Hannun, Y. A. *EMBO Rep.* **2004**, *5*, 777−782.
(2) Ballou, L.; Lauledерkind, S.; Rosloniec, E.; Raghow, R. *Biochim. Biophys. Acta* **1996**, 1301.
(3) Merrill, A. H.; Schmelz, E. M.; Dillehay, D. L.; Spiegel, S.; Shayman, J. A.; Schroeder, J. J.; Riley, R. T.; Voss, K. A.; Wang, E. *Toxicol. Appl. Pharmacol.* **1997**, *142*, 208−225.
(4) Peña, L. A.; Fuks, Z.; Koksnick, R. *Biochem. Pharmacol.* **1997**, *53*, 615−621.
(5) Harouse, J. M.; Bhat, S.; Spitalnik, S. L.; Laughlin, M.; Stefano, K.; Silberberg, D. H.; Gonzalez-Scarano, F. *Science* **1991**, *253*, 320−323.
(6) Van Berg, L. H. D.; Sadiq, S. A.; Lederman, S.; Latov, N. *J. Neurosci. Res.* **1992**, *33*, 513−518.

(7) Fishman, P. H.; Pacuszka, T.; Orlandi, P. A. *Adv. Lipid Res.* **1993**, *25*, 165−87.
(8) Hannun, Y. A.; Obeid, L. M. *Nat. Rev. Mol. Cell Biol.* **2008**, *9*, 139−150.
(9) Jayadev, S.; Liu, B.; Bielawska, A. E.; Lee, J. Y.; Nazaire, F.; Pushkareva, M. Y.; Obeid, L. M.; Hannun, Y. A. *J. Biol. Chem.* **1995**, *270*, 2047−2052.
(10) Kolesnick, R. *J. Clin. Invest.* **2002**, *110*, 3−8.
(11) Merrill, A. H. *J. Biol. Chem.* **2002**, *277*, 25843−25846.
(12) Rowat, A. C.; Kitson, N.; Thewalt, J. L. *Int. J. Pharm.* **2006**, *307*, 225−231.
(13) Megha,; Sawatzki, P.; Kolter, T.; Bittman, R.; London, E. *Biochim. Biophys. Acta, Biomembr.* **2007**, *1768*, 2205−2212.
(14) Sot, J.; Bagatolli, L. A.; Goñi, F. M.; Alonso, A. *Biophys. J.* **2006**, *90*, 903−914.
(15) Slotte, J. P. *Chem. Phys. Lipids* **1999**, *102*, 13−27.
(16) Waxman, S. G.; Ritchie, J. M. *Ann. Neurol.* **1993**, *33*, 121−136.
(17) Ariga, T.; Jarvis, W. D.; Yu, R. K. *J. Lipid Res.* **1998**, *39*, 1−16.
(18) Zhang, Y.; Kolesnick, R. *Endocrinology* **1995**, *136*, 4157−4160.
(19) Kanety, H.; Feinstein, R.; Papa, M. Z.; Hemi, R.; Karasik, A. *J. Biol. Chem.* **1995**, *270*, 23780−23784.
(20) Singh, I.; Pahan, K.; Khan, M.; Singh, A. K. *J. Biol. Chem.* **1998**, *273*, 20354−20362.
(21) Huang, H. W.; Goldberg, E. M.; Zidovetzki, R. *Biochem. Biophys. Res. Commun.* **1996**, *220*, 834−838.
(22) Thewalt, J.; Kitson, N.; Araujo, C.; MacKay, A.; Bloom, M. *Biochem. Biophys. Res. Commun.* **1992**, *188*, 1247−1252.
(23) Sot, J.; Aranda, F. J.; Collado, M. I.; Goñi, F. M.; Alonso, A. *Biophys. J.* **2005**, *88*, 3368−3380.
(24) Pandit, S. A.; Scott, H. L. *J. Chem. Phys.* **2006**, *124*, 014708.
(25) Xu, X.; Bittman, R.; Duportail, G.; Heissler, D.; Vilcheze, C.; London, E. *J. Biol. Chem.* **2001**, *276*, 33540−33546.
(26) Wang, J.; Megha; London, E. *Biochemistry* **2004**, *43*, 1010−1018.
(27) Megha,; London, E. *J. Biol. Chem.* **2004**, *279*, 9997−10004.
(28) Busto, J. V.; Sot, J.; Requejo-Isidro, J.; Goñi, F. M.; Alonso, A. *Biophys. J.* **2010**, *99*, 1119−1128.
(29) Hsueh, Y. W.; Giles, R.; Kitson, N.; Thewalt, J. *Biophys. J.* **2002**, *82*, 3089−3095.
(30) Pandit, S. A.; Chiu, S. W.; Jakobsson, E.; Grama, A.; Scott, H. L. *Biophys. J.* **2007**, *92*, 920−927.
(31) Chiu, S. W.; Vasudevan, S.; Jakobsson, E.; Mashl, R. J.; Scott, H. L. *Biophys. J.* **2003**, *85*, 3624−3635.
(32) Zhang, Z.; Bhide, S. Y.; Berkowitz, M. L. *J. Phys. Chem. B* **2007**, *111*, 12888−12897.
(33) Megha,; Bakht, O.; London, E. *J. Biol. Chem.* **2006**, *281*, 21903−21913.
(34) Nose, S.; Klein, M. *Mol. Phys.* **1983**, *50*, 1055−1076.
(35) Shah, J.; Atienza, J. M.; Duclos, R. I.; Rawlings, A. V.; Dong, Z.; Shipley, G. G. *J. Lipid Res.* **1995**, *36*, 1936−1944.
(36) Berendsen, H. J. C.; van der Spoel, D.; van Drunen, R. *Comput. Phys. Commun.* **1995**, *91*, 43−56.
(37) Lindahl, E.; Hess, B.; van der Spoel, D. *J. Mol. Model.* **2001**, *7*, 306−317; 10.1007/s008940100045.
(38) Hess, B.; Bekker, H.; Berendsen, H. J. C.; Fraaije, J. G. E. M. *J. Comput. Chem.* **1997**, *18*, 1463−1472.
(39) Essmann, U.; Perera, L.; Berkowitz, M. L.; Darden, T.; Lee, H.; Pedersen, L. G. *J. Chem. Phys.* **1995**, *103*, 8577−8593.
(40) Parrinello, M.; Rahman, A. *J. Appl. Phys.* **1981**, *52*, 7182−7190.
(41) Pandit, S. A.; Jakobsson, E.; Scott, H. L. *Biophys. J.* **2004**, *87*, 3312−3322.
(42) Nagle, J. F.; Tristram-Nagle, S. *Biochim. Biophys. Acta, Rev. Biomembr.* **2000**, *1469*, 159−195.
(43) Niemelä, P.; Hyvönen, M. T.; Vattulainen, I. *Biophys. J.* **2004**, *87*, 2976−2989.
(44) Khelashvili, G. A.; Scott, H. L. *J. Chem. Phys.* **2004**, *120*, 9841−9847.
(45) Petrache, H. I.; Feller, S. E.; Nagle, J. F. *Biophys. J.* **1997**, *72*, 2237−2242.
(46) Mehnert, T.; Jacob, K.; Bittman, R.; Beyer, K. *Biophys. J.* **2006**, *90*, 939−946.
(47) Greenwood, A. I.; Tristram-Nagle, S.; Nagle, J. F. *Chem. Phys. Lipids* **2006**, *143*, 1−10.
(48) Edholm, O.; Nagle, J. F. *Biophys. J.* **2005**, *89*, 1827−1832.
(49) Douliez, J.; Léonard, A.; Dufourc, E. *Biophys. J.* **1995**, *68*, 1727−1739.
(50) Ryabova, N.; Kiselev, M.; Balagurov, A. *Crystallogr. Rep.* **2010**, *55*, 479−487; 10.1134/S1063774510030193.
(51) Jensen, J.-M.; Schutze, S.; Neumann, C.; Proksch, E. *J. Invest. Dermatol.* **2000**, *115*, 708−713.
(52) Busto, J. V.; Fanani, M. L.; De Tullio, L.; Sot, J.; Maggio, B.; Goñi, F. M.; Alonso, A. *Biophys. J.* **2009**, *97*, 2717−2726.
(53) Huang, J.; Feigenson, G. W. *Biophys. J.* **1999**, *76*, 2142−2157.
(54) Kell, G. S. *J. Chem. Eng. Data* **1975**, *20*, 97−105.
(55) Errington, J. R.; Panagiotopoulos, A. Z. *J. Phys. Chem. B* **1998**, *102*, 7470−7475.